Characterization of the size and orientation of Na and Cl-2 nanocrystals in electron irradiated NaCl crystals by means of synchrotron radiation

Sulyanov, S. N.; Kheiker, D. M.; Dorovatovskii, P. V.; Sugonyako, A. V.; Vainshtein, D. I.; den Hartog, H. W.

Published in:
Journal of Physics-Condensed Matter

DOI:
10.1088/0953-8984/19/24/246210

Document Version
Publisher's PDF, also known as Version of record

Publication date:
2007

IOP PUBLISHING JOURNAL OF PHYSICS: CONDENSED MATTER

J. Phys.: Condens. Matter **19** (2007) 246210 (12pp) doi:10.1088/0953-8984/19/24/246210

Characterization of the size and orientation of Na and Cl_2 nanocrystals in electron irradiated NaCl crystals by means of synchrotron radiation

S N Sulyanov[1,2], D M Kheiker[1,2], P V Dorovatovskii[1,2], A V Sugonyako[3], D I Vainshtein[3] and H W den Hartog[3,4]

[1] Institute of Crystallography, RAS, 119333, Leninsky Prospekt 59, Moscow, Russia
[2] Kurchatov Centre of Synchrotron Radiation and Nanotechnology, 123182, Kurchatova ploshad 1, Moscow, Russia
[3] University of Groningen, Nijenborgh 4, NL-9747 AG Groningen, The Netherlands

E-mail: lrd942@ns.crys.ras.ru (S V Sulyanov), kheiker@ns.crys.ras.ru, paulgemini@mail.ru (P V Dorovatovskii), a.v.sugonyako@rug.nl, d.i.vainchtein@rug.nl and h.w.den.hartog@rug.nl

Received 19 December 2006, in final form 2 May 2007
Published 22 May 2007
Online at stacks.iop.org/JPhysCM/19/246210

Abstract

Samples of synthetic NaCl crystals have been exposed to doses of electron irradiation up to 10^{-2} TGy (1 Trad) at about 100 °C, and studied subsequently at $T = 95$ K by means of synchrotron radiation (SR). In addition to the earlier established Kurdjumov–Sachs orientation relationship (K–S OR) for Na precipitates, the following OR is revealed between solid chlorine and the host NaCl crystal system: $\{001\}_{Cl} \parallel \{001\}_{NaCl}$, $\langle 110\rangle_{Cl} \parallel \langle 110\rangle_{NaCl}$. The size and shape of the Cl_2 precipitates has been studied as a function of the amount of radiation damage (i.e. the concentrations of Na and Cl_2).

(Some figures in this article are in colour only in the electronic version)

1. Introduction

Information from a variety of independent experiments (e.g. differential scanning calorimetry (DSC), electron paramagnetic resonance (EPR), AC conductivity, nuclear magnetic resonance (NMR), optical absorption spectroscopy, Raman scattering, and atomic force microscopy) has shown that during exposure of NaCl to ionizing radiation at elevated temperatures (e.g. 100 °C), with increasing dose increasing amounts of metallic Na and chlorine bubbles are formed [1–11]. Until now the physical properties of the metallic Na precipitates have been studied most extensively, and these investigations have shown that quite often the Na nanoparticles behave anomalously. These results suggest that in heavily damaged NaCl the Na precipitates are

[4] Author to whom any correspondence should be addressed.

complex systems consisting of small individual building blocks with diameters of a few nanometres.

It is well known that the melting behaviour of very small particles depends sensitively on the particle size [2, 3, 12]. In the case of particles with complex geometrical shapes it appears that the key property is the average local radius of the precipitate system [12]. We have obtained independent information from a variety of experimental investigations that the precipitate structures are best described by conglomerates of very small particles with dimensions of a few nanometres [4, 5, 7, 12]. These conglomerates are very interesting from a scientific point of view, because they show exciting specific heat effects as a result of their reduced stability of the local geometrical properties [12]. In addition, the optical absorption properties and Raman scattering results have revealed that we are dealing with (fractally shaped) clusters consisting of very small particles showing appreciable spill-out of the conduction electrons [3, 14] and properties which are associated with the quasi-1D nature of the Na precipitate system [1, 10]. Finally, we note that AC conductivity and capacitance measurements have shown that for heavily damaged NaCl at some temperature the conductivity increases dramatically with increasing amount of Na (>1 at.%) and the width of the dielectric loss peak decreases with increasing Na%. At sufficiently high concentration both the conductivity and the capacitance show critical behaviour, which can be explained in terms of a transition of reasonably localized electronic motion in moderately damaged samples (<1 at.% Na) to long-range electronic conductivity in highly connected (quasi-1D) systems of Na nano-particles [4]. Direct observations showing strong evidence for these complex structures have been obtained from atomic force microscopy (AFM) experiments [13].

So far radiolytic chlorine precipitates in NaCl have been studied by means of latent heat measurements of melting (LHM) and (LHF) freezing processes at low temperatures, in the vicinity of the triple point of chlorine (−101 °C). The melting and solidification results are different: the LHF peak of radiolytic chlorine is located about 20 °C below the triple point, while the value for the LHF is about 9% less than the LHM (LHF ∼ 1.09 LHF). Both effects can be explained simultaneously by assuming that the pressure in the chlorine bubbles is about 0.1 GPa. As mentioned below, the pressure estimated from the specific volume of the Cl_2 precipitates is a factor of six larger. It is not unexpected that different methods to calculate the internal pressure yield different results, because the calculations are based on the assumption that the relevant thermodynamic properties of the nano-precipitates are the same as for bulk Cl_2, which is of course not certain.

Earlier [15] we used x-ray diffractometers with 2D-area detectors to study samples of synthetic NaCl ($Fm\bar{3}m$), which had been irradiated by 0.5 MeV electrons. K–S OR was revealed and the Na ($Im\bar{3}m$) precipitate size was estimated by the Scherrer formula in the spherical approximation. Recently, we have presented our first combined x-ray, Na and Cl_2 melting results for both Na and Cl_2 precipitates and conduction electron spin resonance results of Na nano-particles in heavily damaged NaCl in a short paper [16].

The system Li–Li_2O was studied in [17]. Judging by the designations of the OR used, we can note that the difference between an ideal K–S OR for which the rotation angle is $\Theta = 5.26°$ and the special value characterizing the fcc/bcc geometry is $r = 1.0887$ (see [15, 18, 19]) and the published value of 4.4° ($r = 1.073$ for Li–Li_2O; Li_2O has an fcc lattice) is small. A Nishiyama–Wasserman OR ($\Theta = 0°$) was revealed for the system Li–LiH [20]. The size of Li precipitates in LiH crystals with 10 at.% Li was estimated as not less than about 500 Å. The accuracy was restricted by the angular resolution of the instrument.

In this study NaCl samples, exposed to radiation doses between 0.15 and 1.0 Trad, and containing 1.0–21.0 vol.% Na (obtained from DSC data), were studied with SR at either $T = 95$ or 300 K. The main purpose of the present work was to measure the OR for the frozen Cl_2

(*Cmca*) precipitates and to refine the size determination of both Na and Cl_2 precipitates by means of high resolution SR in wide angles. We will present dependable results for the amounts of Na and Cl_2, while new, interesting information on the size and shape of these precipitate systems is also obtained. With increasing irradiation dose (and increasing damage) the sizes of both precipitate systems (which are of the same order of magnitude) increase.

2. Experimental details

2.1. Sample preparation, irradiation and characterization

The NaCl samples used for this investigation have been prepared in a pure He atmosphere in carbon crucibles, by means of a modified Bridgman technique using a high frequency furnace. The impurities (KCl or KBF_4) were added to the raw NaCl material prior to crystal growth. The diameter of the cylindrical single crystals was 6 mm and thin disk shaped samples with a thickness of 0.5 mm were cut from the boules and polished afterwards. As many as 300 of these samples can be accommodated in the sample holder with a surface area of about 300 cm^2, which is irradiated in vacuum by 0.5 MeV electrons from a linear accelerator. The samples were irradiated at temperatures between 50 and 150 °C, and doses up to 10^{-2} TGy (1 Trad) have been used for the present investigations.

To characterize the samples we have carried out latent heat measurements with a Perkin Elmer DSC-7 calorimeter set-up. The latent heat of melting of the metallic Na precipitates provides information about the amount of radiolytic Na in the sample [3]. We note that the melting temperature of bulk Na is about 97 °C, whereas the latent heat peak of melting associated with radiolytic Na in NaCl is often at a different position, probably due to size effects [3]. Several samples have been investigated—also for the purpose of characterization—by means of DSC at low temperature using a Perkin Elmer low temperature measuring head in conjunction with the above mentioned calorimetry set-up to establish the presence of chlorine precipitates.

2.2. The single crystal experiments

We have used the 'Belok' station installed in the source from the bending magnet in the Kurchatov Centre of Synchrotron Radiation and Nanotechnology (KCSR, Moscow, Russia) [21] for the single crystal experiments. The station is based on a MAR CCD detector operating in the 2048 × 2048 pixel resolution mode. The samples used for this investigation were cleaved and had an oblong shape, with a diameter in the range 0.15–0.3 mm. During the experiment they were glued by one end on the holder, such that the incident beam did not touch the cement during the exposure to minimize the background scattering. The samples were mounted approximately along the horizontal ϕ-axis of the goniometer. For $\lambda = 1.5398$ Å the $I(\lambda/2)$ contribution from the white spectrum cannot be removed totally by the segmented mirror, but this intensity did not exceed about 3×10^{-3} times the intensity of the main line $I(\lambda)$. During the exposures the detector was set higher than the incident beam such that the width of the range of scattering angles, which are between $2\theta_{\min}$ and $2\theta_{\max}$, and where simultaneous registration was carried out, was 25°. 180 successive patterns with ϕ-steps of 1° and 2 min exposure each were registered. During each exposure the sample was rotated within $\Delta\phi = \pm 0.5°$ to average the intensity. The diffraction patterns were processed later on. The 'stellar sky' type CCD specific detector background features were removed by a special treatment utilizing couples of patterns obtained under the same conditions. The laboratory coordinates were chosen such that the x-axis was directed along the horizontal ϕ-rotation axis.

The orientation matrix (OM) **A** for the host crystal ($\mathbf{r}_{\mathrm{NaCl}} = \mathbf{A}\mathbf{n}_{\mathrm{NaCl}}$ and $\mathbf{n}_{\mathrm{NaCl}} = \mathbf{A}_{\mathrm{NaCl}^{-1}}\mathbf{r}_{\mathrm{NaCl}}$, where any unit vector coordinates are considered in the laboratory, **r**, and crystallographic unit basis, **n**) was calculated as in [15] via three Eulerian angles. All vectors registered from the Na and Cl_2 precipitates were considered in the NaCl coordinate system after the $\mathbf{A}_{\mathrm{NaCl}^{-1}}$ transformation. Any matrix connecting the host crystal and precipitate can be chosen from a set of equivalent matrices, the number of these depending on the host crystal symmetry. Each one from this set can be obtained by multiplying OM by a matrix $\mathbf{W}_i$ representing one of the point group rotation operators for the crystal under investigation. Any reciprocal vector $\mathbf{g}_{\mathrm{prec}}$ of the precipitate can be written via its direction cosines ($\mathbf{g}_{\mathrm{NaCl}}$) in NaCl unit basis coordinates as $\mathbf{g}_{\mathrm{prec}} = \mathbf{W}_i\mathbf{U}\mathbf{g}_{\mathrm{NaCl}}$ ($i = 1, N_w$). Here $N_w = 24$ for the point group $m\bar{3}m$ and **U** is any matrix connecting NaCl and precipitate systems. (It should be noted here that in the case of a non-cubic precipitate lattice one should consider all vectors in a unit basis connected with the crystal basis by the proper transformation matrix. We did not use this approach here and described the OR by crystallographic symbols of planes and directions; see below.) If p is the multiplicity factor for a particular crystallographic coordinate plane of the precipitate, and N_w is the number of $\mathbf{W}_i$-matrices for the host crystal, then the maximum number of possible reflections in the diffraction pattern is $P = pN_w$. In particular cases of OR some of the $\mathbf{W}_i$-matrices may result in equivalent transformations, so the number of possible reflections is reduced. Thus there are only 12 matrices, resulting from non-equivalent transformations associated with the Nishiyama–Wasserman OR [20], and the same applies to our case of the solid Cl_2–NaCl OR (see below). It turned out that all Na [15] and all molecular Cl_2 precipitate reflection vectors measured within their sets had equivalent orientations and were connected by $\mathbf{W}_i$-matrices.

We have obtained the instrumental resolution function (IRF) in the following way. We have used a reference powder (zeolite or LaB_6 N660a NIST standard) inserted into a glass capillary with an inner diameter of $D = 0.3$ mm. When the sample-to-detector distance is $R_0 = 380$ mm, the expected angular resolution is $\Delta(2\theta) = D/R_0 = 0.045°$, assuming that the incident beam is approximately parallel. By averaging the intensity over the whole detector plane, using the method described in [22], we have obtained the dependence of the intensity on the scattering angle [$I(2\theta)$]. The FWHM of the Bragg peaks in this case shows a very weak dependence on 2θ in the region used and its value is 0.055°, while the mean angular difference between the measured and the reference Bragg angles did not exceed 0.001°. A slight increase of the width is mainly due to technical causes such as pixel size of the detector (0.08 mm), and the angular divergence of the incident beam in the horizontal plane (especially at lower Bragg angles [22]). The vertical divergence is negligible. The peak profile of the IRF is well described by the symmetric Pearson-VII (PVII) or the pseudo-Voigt (pV) function (see figure 1).

A special routine was used to treat the weak reflections from the precipitates. This method was particularly crucial for the observation of very weak Bragg spots obtained for the crystals with the lowest percentages of radiation damage, i.e. with the lowest precipitate volume concentrations. Each reflection was surrounded by a region which in general was chosen wider along the anti-Bragg direction where the reflection showed a wider spread, implying that it was relevant to assume axial symmetry about the incident beam within the region. We have adopted here the same approach as in [22], used to treat the diffuse peaks obtained for liquid crystals, i.e. we have processed the pixel intensities to calculate the $I(2\theta)$ dependence. This method allows one to evaluate the real peak shape along the Bragg direction and at the same time the statistical counting errors in the profile points are diminished substantially. Sometimes it was possible to recover the peak shape even if the averaged intensity exceeded the background only by one to two counts/pixel. Each peak thus obtained was used further for fitting by PVII and pV functions, which gave about the same results for the value of FWHM. It should be

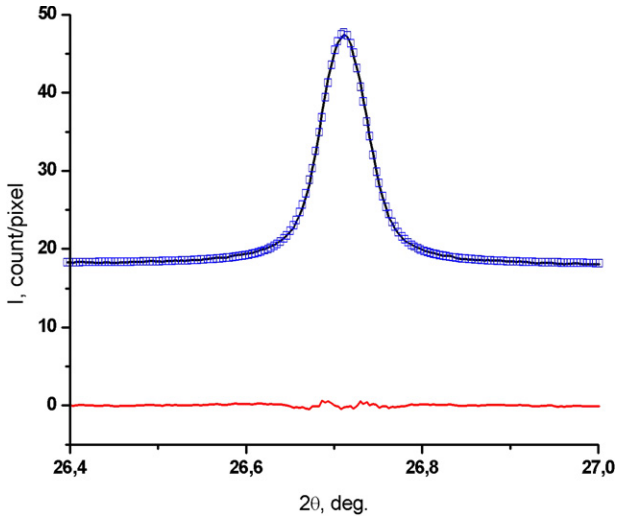

Figure 1. Bragg peak (642) from zeolite powder, its interpolation by the Pearson-VII function and the difference between measured and calculated values.

noted that, as the cleaved sample size was slightly different from sample to sample, the precise IRF definition in each case was quite difficult. The deconvolution procedure with the IRF should be used to evaluate the physical (size and strain) line broadening for the precipitates. In most cases the peaks associated with the precipitates were substantially wider than the maximum possible value for the IRF and so we applied the simplified procedure to calculate the physical broadening, i.e. we used a constant reference value of the FWHM for all reflections and assumed that the measured and reference profiles were described by a squared Lorentzian (Cauchy) function. Our approach was relevant for all Na reflections and for Cl_2 reflections at lower Na percentage. We emphasize that better angular resolution is necessary for more accurate measurement of the host NaCl peaks and also for peaks from larger Cl_2 precipitates at highest doses. Also note that the irregular shape of the cleaved samples made it difficult to allow for a proper absorption correction for a particular peak as the radiation used had low energy. Due to this the accuracy of the precipitate volume percentage measurement decreases.

2.3. The powder experiments

We have also performed powder experiments in order to obtain estimates for the volume percentages of the three phases present in the samples (i.e. NaCl, Na, and Cl_2). The single crystal samples were crushed in a mortar to about 30 μm grain size (this quite large size was used to avoid serious interaction between the precipitates in the NaCl host crystal and the surrounding atmosphere). After this the coarse grain powder was inserted into a glass capillary with a diameter of 0.3 mm. The capillary was rotated about the horizontal ϕ-axis during exposure. The procedure described in [22] was applied to calculate $I(2\theta)$. We used the peak intensities of the three phases obtained by profile fitting for the calculations. It was difficult to use the standard full profile Rietveld method, because of the non-standard Cl_2 and Na peak shape dependence as a function of 2θ.

3. Results and discussion

The orthorhombic unit cell and the atomic structure of crystalline molecular chlorine was described in [23]. The unit cell is depicted in figure 2. We have obtained the peak profile

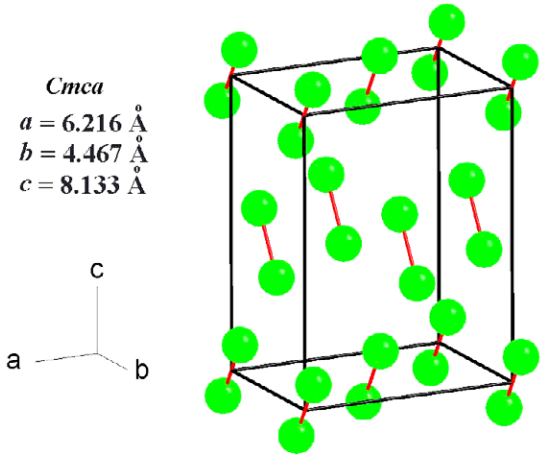

Figure 2. Molecular chlorine crystal structure.

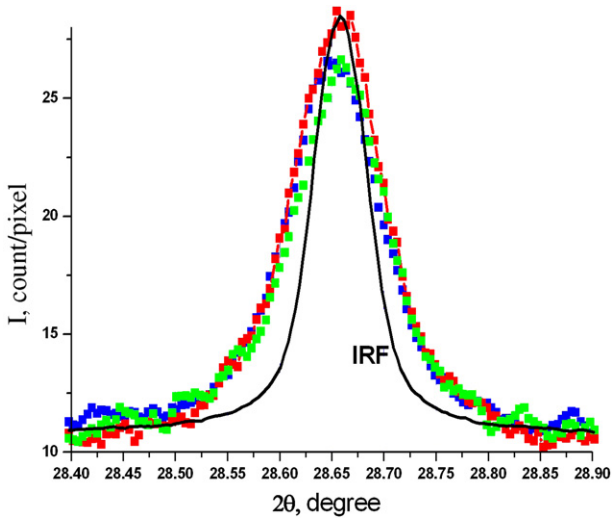

Figure 3. 200-peaks from Cl_2 precipitates and instrumental resolution function.

parameters as explained above for different systems of indices. The parameters showed quite good reproducibility. For example, for six Cl_2 precipitate reflections of the 200 type (the multiplicity factor is 2, so 2×12 reflections are possible), corresponding to different $\mathbf{W}_i$-matrices, obtained for sample 3 (table 1), the averaged values obtained by pV function fitting were $2\theta = 28.660(13)^\circ$ and the FWHM was $\Delta(2\theta) = 0.140(9)^\circ$. Several 200-type peaks are presented in figure 3.

We have measured the lattice parameters for Cl_2 precipitates at $T = 95$ K. Peak centroids were used to obtain asymmetric peak positions. The measured averaged values are $a = 6.216(3)$, $b = 4.467(9)$, $c = 8.133(9)$ Å. The spread for samples 1–4 is in brackets. The corresponding (less accurate) literature values are $a = 6.24$, $b = 4.48$, $c = 8.26$ Å. The cell volume in our case is 97.8% of the published value. Judging by the volume–pressure dependence [24] we estimate the inner pressure to be about 0.6 GPa.

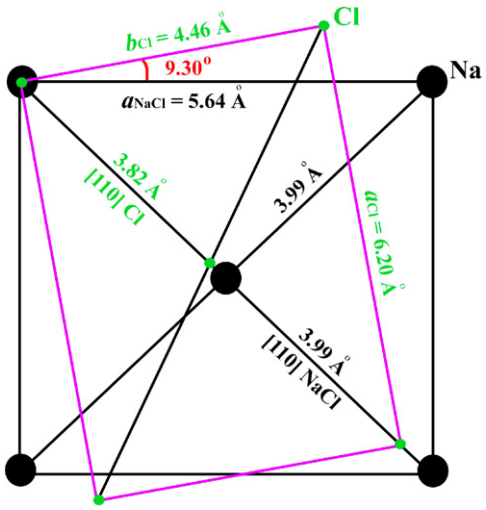

Figure 4. Orientation relationship for Cl_2–NaCl system. Knots of Cl_2 and NaCl crystal lattice are designated.

Table 1. Samples studied.

Sample number and vol.% Na (DSC)	Dose (Trad)	Dose rate (Mrad h^{-1})	T (°C)	Estimated (volume averaged) Cl_2 precipitate size L_{hkl}, (Å)		Estimated Cl_2 precipitate size model as from ellipsoid $V^{1/3}$ (Å)	Estimated (volume averaged) Na precipitate size, L_{110} (Å)	Vol.% Na (x-ray data)
				Along c, 002	Along a, 200			
(1) 1.0	0.15	250	60	190	470	310(60)	200(50)	1.1[a]
(2) 2.86	0.15	250	100	310	830	420(100)	370(40)	3.5
(3) 9.33	0.15	100	100	340	830	450(110)	450(50)	7.1
(4) 16.15	1.0	500	100	460	1070	830(190)	580(60)	10.3
(5) 21.27	1.0	500	100	—	—	—	690(80)	—

[a] Lower accuracy data because of the peak weakness.

The following OR was revealed for chlorine precipitates: $\{001\}_{Cl} \parallel \{001\}_{NaCl}$; $\langle 110\rangle_{Cl} \parallel \langle 110\rangle_{NaCl}$ within the accuracy of our measurements (about 0.3°). The OR of chlorine precipitates in the NaCl host crystal is shown in figure 4. The rotation angle for $\langle 100\rangle_{Cl}$ around $\langle 100\rangle_{NaCl}$ found in the experiment is 9.1° while the angle calculated from the measured cell parameters which is required for the coincidence of the cubic and orthorhombic cell diagonals is 9.3° (see also figure 5). Note that the inter-atomic spaces in the rows $\langle 110\rangle_{Cl}$ and $\langle 110\rangle_{NaCl}$, which are equal to 3.82 Å and 3.99 Å respectively, differ by less than 4.5%, which means that the atomic positions in these rows reveal a slight misfit. Our precipitate system is more complex than those encountered in the literature, which deal for example with epitaxial growth or with the metal precipitates in metallic host crystals. Our Cl_2–NaCl system is three dimensional, and the host crystal (with ionic bonding) consists of two sub-lattices with different charges, while in the precipitate we are dealing with covalent molecular bonds. We assume, however, that the crystal lattices of both the metallic (Na) and molecular (Cl) nanocrystal precipitates at their interfaces with the host matrix conform to the ionic NaCl crystal sub-lattices.

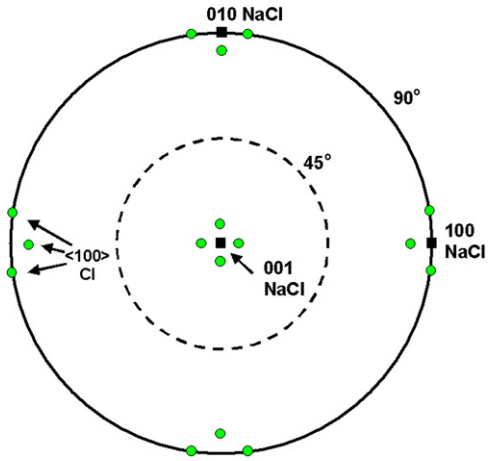

Figure 5. Projection of the ⟨100⟩ directions of Cl_2 precipitates in the unit cell coordinate system of an ideal NaCl crystal. The directions ⟨001⟩Cl_2 and ⟨100⟩ NaCl coincide.

In the analysis of the Bragg peaks from the Cl_2 precipitates, one should take into account that the shape of a particular reflection, obtained for one of the 12 possible orientations, corresponds to the averaged intensity from precipitates, which may show a certain spread in the distribution of sizes and shapes. It turns out that the shape of the Cl_2 precipitates is not spherical, which can be concluded from the observed differences of the widths of the Bragg peaks. Thus, for the samples studied the 002 Cl_2 peaks are at least twice as wide as the 200 Cl_2 peaks, even though the Bragg angles do not differ much. This can be explained by a substantially reduced precipitate size along the crystal c-axis. In this experiment with the wavelength used we were not able to obtain diffraction patterns which were richer in reflections. So, we were not able to observe the reflections with at least doubled indices, which are required if we want to reliably separate the contribution to the broadening from the size and strain effects. Quite a number of factors may result in anisotropic line broadening; see for example [25]. Let us dwell here on the three-axial ellipsoid model proposed in [26]. In our particular case, we are dealing with three-axial ellipsoids oriented relative to the host NaCl crystal lattice. The ellipsoid equation was written in reciprocal space. If L_{hkl} is the volume averaged domain size along $[hkl]$, then the proposed expression is

$$L_{hkl} = (3/2)/(b_{11}h^2 + b_{22}k^2 + b_{33}l^2 + b_{12}hk + b_{13}hl + b_{23}kl)^{1/2}d_{hkl},$$

where d_{hkl} is the interplanar distance, and the ellipsoid radii along a, b, c-axes are connected with the L-values, i.e. $r_{a,b,c} = (2/3)L_{a,b,c}$. In our particular case of precipitates with an orthorhombic cell, the values b_{12}, b_{13}, b_{23} are zero. So, the values b_{11}, b_{22}, b_{33} should be refined taking properly into account the widths of all reflections, measured by means of a least-squares fitting method after IRF deconvolution. An example of such a refinement for sample 2 is presented in table 2. The calculated ellipsoid sizes are $r_a = 560$, $r_b = 200$, $r_c = 160$ (Å) (the volume is $V = (4/3)\pi r_a r_b r_c$). The mean absolute deviation is 100 Å. We suppose such a discrepancy can give us a certain error estimation, but it is seen also that, although this model has a certain relevance, it cannot be considered to be really appropriate in our case. The trend of the differences between the measured and model values is similar for other Na concentrations. We suppose that both the size and strain anisotropy should be taken into account to describe the precipitates more accurately. In this case a substantially larger number of reflections is required. We put as benchmarks the L_{hkl} values measured by 002 and 200 reflections in table 1. This

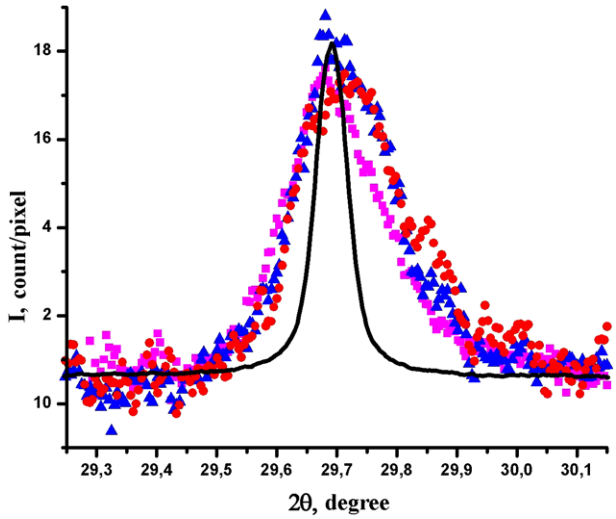

Figure 6. 200 peaks from Na precipitates and instrumental resolution function.

Table 2. Volume averaged Cl_2 precipitate size measured by physical line broadening, estimated by the ellipsoid model, and their difference for sample 2 (see table 1). The mean absolute deviation is 100 Å.

hkl	L_{hkl} measured (Å)	L_{hkl} model estimation (Å)	ΔL_{hkl} (Å)
002	310	250	60
111	460	330	130
200	830	840	−10
112	610	290	320
202	380	380	0
113	160	270	−110
021	220	290	−70

treatment yields a monotonic increase of the size of the precipitates with increasing radiation damage up to 16 vol.% Na.

We could measure only the first two types of reflections for Na, i.e. 110 and 200, with good resolution, the second one being weak. The lack of experimental information makes it difficult to discern between the size and strain effects. But we note that the 200 peaks were substantially wider and this could not be referred only to the $1/\cos\theta$ multiplier. The peaks have a certain asymmetry (see figure 6), though they can be described quite well by a symmetric function as a first approximation. This asymmetry can be caused by lattice parameter distribution in the precipitates, which may have a certain size distribution. The estimated size of the Na precipitates is plotted against the vol.% Na (obtained from latent heat of melting experiments for metallic Na) in figure 7. The dependence is monotonic and shows that the radius of these precipitates increases with the concentration of Na. The error bars shown are obtained from the peak widths spread from different peak fitting measurements, taking into account possible errors caused by improper peak profile description.

The Bragg peaks from the host NaCl crystal do not manifest notable broadening, while they do not show any notable change of the lattice parameter up to highest radiation doses either. We think one should use a diffractometer system with even better instrument resolution

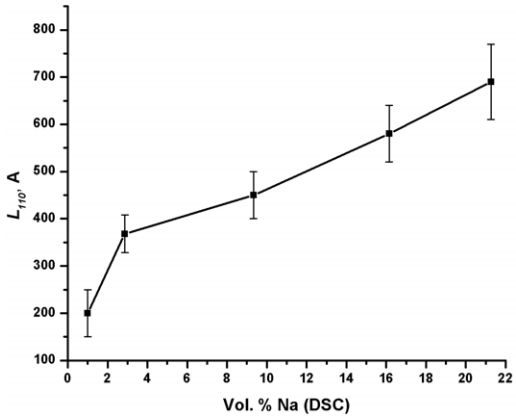

Figure 7. Volume averaged size for Na precipitates (L_{110}) plotted against Na vol.% (DSC data).

to observe the deviations of the NaCl structure caused by irradiation, which resulted in the presence of 10–20%Na and Cl_2! This result is quite exceptional in view of the extremely high percentages of precipitates in these samples. Many other heavily damaged materials show appreciable structural differences compared with their undamaged counterparts. Some heavily damaged ionic materials are even transformed during irradiation into some kind of amorphous state (metamictization).

We have calculated the volume percentages of Na and Cl_2, obtained by the powder method, and the values are in a good agreement with the DSC data (table 1). We have also calculated the atomic percentages of the Cl_2 and Na precipitates and they turned out the same with a maximum error of 20%, which implies that the number of atoms in both types of precipitates is about the same.

It is now interesting to compare the results obtained from x-ray diffraction, reported in this paper, with those found earlier by means of other techniques (ESR, NMR, DSC, and Raman scattering). We note that in those cases where the absolute concentrations of the precipitates could be obtained, there is reasonable agreement with the corresponding values found by means of x-ray diffraction. This implies that the majority of the defects studied with the various experimental techniques are the same and we can exclude the possibility that by means of different techniques entirely different sub-sets of defects are studied. It should be concluded that eventually apart from small numbers of very minute and isolated precipitates, which on one hand do contribute to the melting peaks while in the x-ray study they contribute to the diffuse scattering, we have been looking at the same defects with a variety of experimental techniques.

It is important to note here that the sizes of the radiation-induced Na and Cl_2 precipitates, obtained by means of the high-resolution x-ray diffraction experiments, are much larger than those estimated from earlier investigations with other techniques [1–11]. In contrast with the 'x-ray sizes' in the range of several hundred angstroms, presented in tables 1 and 2, the results obtained with the other techniques suggest that the average size of the precipitates is a few dozen angstroms, which means that there is a discrepancy of at least one order of magnitude.

The melting properties of the precipitates are determined in the first place by the local geometry of the precipitates, including the curvature of detailed parts of the interface between the precipitates and the host matrix. In the case of strong curvature, which means that the effective size of the precipitates is very small, the melting temperature of the corresponding part of the precipitates is affected significantly. From the experimental observations, showing

that the latent heat effect is dominated by an anomalous melting peak and does not reveal a trace of the features of bulk Na melting, we conclude that due to the interactions with the NaCl host crystal at nano-scale the precipitated phase of Na in very heavily damaged NaCl differs from bulk Na. Also the ESR, NMR and Raman scattering results of Na precipitates are determined by localized effects, occurring at a scale less than the 'x-ray sizes' of these precipitates. In ESR experiments on Na precipitates in heavily damaged NaCl, carried out at room temperature, it seems that the size of the precipitates increases with the dose. Extension of the experiments to low temperatures (between 4 and 300 K) leads to a far more delicate picture. It appears that the system of conduction electrons undergo a metal–insulator phase transition [27]. At high temperature the precipitates behave more or less as reasonably large metallic objects, consisting of many individual nano-particles with sizes of only a few nanometres in diameter, because the conduction electrons are delocalized. At sufficiently low temperature (below the M–I phase transition) the conduction electrons are localized in the very small individual Na nano-precipitates that build the much larger conglomerates and the ESR signal is characterized by conduction electrons located in extremely small individual (but interacting) precipitates. These are the reasons why the detailed results, obtained with ESR, NMR and Raman scattering agree with the melting results.

4. Concluding remarks

- Nanoparticles of metallic Na with sizes of about 200–700 Å and molecular Cl_2 of about 200–1000 Å, depending on the conditions and dose of electron irradiation, are present in the NaCl matrix. With increasing amount of damage, the size of the precipitates increases.
- Cl_2 precipitates show anisotropic line broadening depending on the reflection indices. The precipitate form cannot be described completely by a known ellipsoid model, though it has a certain relevance.
- The x-ray diffraction results presented in this paper provide very interesting information about the overall structure of the precipitate systems. This information is complementary to that obtained earlier by means of DSC, ESR, NMR, and Raman scattering, i.e. methods which probe the local structure of the precipitates.
- All Cl_2 precipitates have the following OR: $\{001\}_{Cl} \parallel \{001\}_{NaCl}$, $\langle 110\rangle_{Cl} \parallel \langle 110\rangle_{NaCl}$.
- The host NaCl crystal Bragg peaks do not show notable broadening up to highest radiation doses.

Acknowledgments

The work was partly financed by the NATO CLG grant EST.NR.CLG 980994 and RFFI grant N04-02-16150, and the state contract N02.438.11.7051 FCNTP I.M.

References

[1] Groote J C, Weerkamp J R W, Seinen J and den Hartog H W 1994 *Phys. Rev.* B **50** 9798–802
[2] Seinen J, Weerkamp J R W, Groote J C and den Hartog H W 1994 *Phys. Rev.* B **50** 9793–7
[3] Weerkamp J R W, Groote J C, Seinen J and den Hartog H W 1994 *Phys. Rev.* B **50** 9781–6
[4] Vainshtein D I, den Hartog H P, Datema H C, Seinen J and den Hartog H W 1995 *Radiat. Eff. Defects. Solids* **137** 73–6
[5] Vainshtein D I and den Hartog H W 1996 *Appl. Radiat. Isot.* **47** 1503–7
[6] den Hartog H W, Groote J C and Weerkamp J R W 1996 *Radiat. Eff. Defects. Solids* **139** 1–19
[7] Kanert O, Schmidt C, Küchler R and den Hartog H W 1997 *Ber. Bunsenges.* **101** 1286–90

[8] den Hartog H W 1999 *Radiat. Eff. Defects. Solids* **150** 167–72
[9] Vainshtein D I and den Hartog H W 2000 *Radiat. Eff. Defects. Solids* **152** 23–7
[10] Shtyrkov E I, Klimovitskii A, den Hartog H W and Vainshtein D I 2002 *J. Phys.: Condens. Matter* **14** 9053–68
[11] Sugonyako A V, Vainshtein D I, Turkin A A and Bukharaev A A 2004 *J. Phys.: Condens. Matter* **16** 785–98
[12] Seinen J, Vainshtein D I, Datema H C and den Hartog H W 1995 *J. Phys.: Condens. Matter* **7** 705–16
[13] Gaynutdinov R, Vainshtein D I, Hak S J, Tolstikhina A and den Hartog H W 2003 *Radiat. Eff. Defects. Solids* **158** 77–82
[14] Seinen J, Groote J C, Weerkamp J W R and den Hartog H W 1994 *Phys. Rev.* B **50** 9787–92
[15] Sulyanov S N, Kheiker D M, Vainshtein D I and den Hartog H W 2003 *Solid State Commun.* **128** 419–23
[16] den Hartog H W, Sugonyako A V, Vainshtein D I, Turkin A A, Sulyanov S N, Kheiker D M and Dorovatovskii P V 2007 *Phys. Status Solidi* c **4** 1079–83
[17] Krexner G, Prem M, Beuneu F and Vajda P 2003 *Phys. Rev. Lett.* **91** 135502–5
[18] Ramirez R, Rahman A and Schuller I K 1984 *Phys. Rev.* B **30** 6208–10
[19] Zangwill A 1996 *Physics at Surfaces* (Cambridge: Cambridge University Press)
[20] Smith G S J 1975 *J. Phys. Chem. Solids* **36** 797–9
[21] Kheiker D M, Kovalchuk M V, Shilin Y N, Shishkov V A, Sulyanov S N, Dorovatovskii P V and Rusakov A A 2007 *Crystallogr. Rep.* **52** 358–64
[22] Sulyanov S N, Popov A N and Kheiker D M 1994 *J. Appl. Crystallogr.* **27** 934–42
[23] Donohue J and Goodman S H 1965 *Acta Crystallogr.* **18** 568–9
[24] Fujihisa H, Fujii Y, Takemura K and Shimomura O 1995 *J. Phys. Chem. Solids* **56** 1439–44
[25] Scardi P and Leoni M 1999 *J. Appl. Crystallogr.* **32** 671–82
[26] Zunic T B and Dohrup J 1999 *Powder Diffract.* **14** 203–7
[27] Cherkasov F G, L'vov S G, Tikhonov D A, den Hartog H W and Vainshtein D I 2002 *J. Phys.: Condens. Matter* **14** 7311–9